Journal of Power Sources 183 (2008) 98–108

Contents lists available at ScienceDirect

Journal of Power Sources

journal homepage: www.elsevier.com/locate/jpowsour

Control-orientated thermal model for proton-exchange membrane fuel cell systems

G. Vasu, A.K. Tangirala*

Indian Institute of Technology-Madras, Chennai 600036, India

ARTICLE INFO

Article history:
Received 11 December 2007
Accepted 25 March 2008
Available online 18 April 2008

Keywords:
Proton-exchange membrane fuel cell
Water pump
Thermal model
Interaction analysis
Stack temperature

ABSTRACT

A lumped parameter dynamic model is developed for predicting the stack temperature, temperatures of the exit reactant gases and coolant water outlet in a proton-exchange membrane fuel cell (PEMFC) system. A dynamic model for a water pump is also developed and can be used along with the thermal model to control the stack temperature. The thermal and water pump models are integrated with the air flow compressor and PEMFC stack current–voltage models developed by Pukrushpan et al. to study the fuel cell system under open and closed-loop conditions. The results obtained for the aforementioned variables from open-loop simulation studies are found to be similar to the experimental values reported in the literature. Closed-loop simulations using the model are carried out to study the effect of stack temperature on settling times of other variables such as stack voltage, air flow rate, oxygen excess ratio and net power of the stack. Further, interaction studies are performed for selecting appropriate input–output pairs for control purpose. Finally, the developed thermal model can assist the designer in choosing the required number of cooling plates to minimize the difference between the cooling water outlet temperature and stack temperature.

1. Introduction

Fuel cells are electrochemical reactors which directly convert chemical energy to electrical energy. Fuel cells are typically classified based on the type of electrolyte used in the cell. The proton-exchange membrane fuel cell (PEMFC) is widely studied and attains its name from the use of a polymer membrane as the electrolyte. Most of the current research and development activity focuses on the PEMFC due to its versatile features such as high power density, relatively fast start-up, and short response times to changes in the power demand.

In automobile applications, an important requirement is that the stack should meet the load demands of a varying profile with short transient times. In this regard, knowledge of the stack in terms of steady state and transient behaviour is of critical importance. The dynamic behaviour of a PEMFC system is strongly dependent on the reactant flows and the water and thermal management. One of the several challenges that arise in the control of a PEMFC system is the level of interaction among these various factors such that an interaction study is necessary [1] to understand the relative importance of these parameters. In fact, water and thermal management have become the key technical challenges for fuel cell technology to be feasible for transportation applications. Proper thermal and water management is in fact, also essential to achieve optimum performance from PEMFC stacks [2,3].

Mathematical models play an important role in supporting the design and enhancing the understanding of the effect of parameters on the performance of the stack and fuel cell auxiliary systems. Studies based on these models are useful for the optimum design and control of a real-time stack. Two modeling approaches can be found in the literature. The first gives rise to what are known as *mechanistic* models [4–6] which use an in-depth knowledge of the electrochemistry, heat transfer and mass transfer that are involved in the fuel cells. Such models explain the fundamental processes occurring in fuel cell systems, and are developed as 1D, 2D and 3D models depending on the assumptions involved therein. These dimensional models for thermal and water management, which are summarized in [7,8], require iterative methods to solve the underlying differential and partial differential equations, thereby making them computationally intensive. In essence, the mechanistic models are suited for *design and optimization* of the individual cell components, rather than for control and monitoring of the stack. The second approach includes models that are based on *empirical* or *semi-empirical* equations which are applied to predict the effect of different input parameters on the *voltage–current* characteristics of the fuel cell [9–11]. When compared with the *mechanistic*

* Corresponding author at: Department of Chemical Engineering, Indian Institute of Technology-Madras, Chennai 600036, India. Tel.: +91 4422574181; fax: +91 4422574152.
E-mail address: arunkt@iitm.ac.in (A.K. Tangirala).

0378-7753/$ – see front matter © 2008 Elsevier B.V. All rights reserved.
doi:10.1016/j.jpowsour.2008.03.087

Nomenclature

A	area (m^2)
C_p	specific heat capacity ($J\,mol^{-1}\,K^{-1}$)
g	gravity constant ($m\,s^{-2}$)
h	heat transfer coefficient ($W\,m^{-2}\,K^{-1}$)
ΔH	heat of reaction ($J\,mol^{-1}$)
I	current (A)
J	moment of inertia ($kg\,m^2$)
k	thermal conductivity of air ($W\,m^{-1}\,K^{-1}$)
L	length of stack (m)
m	mass (kg)
M	molar mass ($mol\,g^{-1}$)
n	number of cells in stack
N	molar flow rate ($mol\,s^{-1}$)
N_{pr}	Prandtl number
PEM	proton-electrolyte membrane
Q	water flow rate ($L\,s^{-1}$)
$\dot{Q}$	energy (W)
Ra	Rayleigh number
T	temperature (K)
V	stack voltage (V)
W	mass flow rate ($kg\,s^{-1}$)

Greek letters

ν	kinematic viscosity ($m^2\,s^{-1}$)
ρ	density ($kg\,m^{-3}$)
ω_r	motor speed (rps)

Subscripts

a	anode
c	cathode
cell	proton-exchange membrane cell
com	combined
con	consumed
elec	electrical energy
H_2	hydrogen
H_2O	Water
in	inlet
l	liquid
latent	latent heat
LMTD	Logarithmic mean temperature difference
max	maximum
mot	motor-pump
N_2	nitrogen
out	outlet
O_2	oxygen
sens	sensible heat
stack	proton-exchange membrane fuel cell stack
theo	theoretical chemical energy
trans	net transfer of water
v	vapour
W	water
0	standard condition

models the physical and electrochemical phenomena are modelled at coarser levels. The semi-empirical models for thermal management of a stack cannot be used directly for control studies due to the implicit forms of the expressions that are used to calculate the stack temperature. From a control perspective, therefore, it is important to develop a model that describes the thermal behaviour of a PEMFC stack with good approximation of the dynamics of stack temperature under various load conditions.

The total thermal energy evolved during operation of a fuel cell is the difference between the chemical energy of H_2–O_2(input) and the electrical energy of the stack (output). This thermal energy is distributed as sensible heat of the coolant and reactants, latent heat during phase change of water and heat loss to the surroundings by convection. Most of the lumped parameter models that have been developed for predicting the stack temperature have considered the sensible heat of cooling water as a sole transport factor of the thermal energy [12,13]. One such simple thermal model of the PEMFC stack was embedded into the ADVISOR vehicle simulation package by group of researchers at NREL [14]. The required inputs and parameters for simulating that model were taken from the ADVISOR package of automotive fuel cell stack driving cycles [15].

A paradigm shift is observed in the work by Yu et al. [16] where the latent heat of water during the phase change of water in the fuel cell, the heat loss to the surroundings, the sensible heat of coolant water and reactants are taken into account to predict the temperatures of the stack, the exit reactant gases and the coolant outlet [16]. In this model, the heat loss to the surroundings by convection is not considered explicitly but rather is modelled in an implicit way. This implicit form again limits the utility of the model for control application.

In the present work, control-orientated system-level dynamic models are developed for (i) stack temperature dynamics by explicitly taking into account the heat loss to the surroundings in addition to the latent heat of vapourization, the sensible heat of coolant water and reactants, and (ii) the centrifugal water pump that is used to control the stack temperature. These models are integrated with first-principle based models of an air flow compressor and the *semi-empirical* voltage–current model of Pukrushpan et al. [17].

The results of the present work offer design ideas to (i) achieve the exit coolant water temperature and near stack temperature and (ii) decrease the settling time of the stack temperature. To the best of the authors' knowledge there has been no work reported in the literature that addresses the development of a control-orientated thermal model. Besides, the water pump sub-system model provides a realistic setting for studying the temperature control problem. The goals of the present work are to

- develop a control-orientated lumped parametric system level model for the stack temperature;
- develop a lumped parametric model for the water pump subsystem;
- design the number of cooling plates required to achieve the cooling water exit temperature close to the stack temperature;
- study the interaction between inputs (compressor motor voltage, motor-pump current) and outputs (air flow rate, stack temperature) using developed thermal and water pump models in conjunction with stack and air flow sub-system models;
- study the effect of stack temperature on the settling times of air flow rate, stack voltage and net power.

This paper is organized as follows. First, the development of a dynamic model of the centrifugal water pump is explained in Section 2. The proposed control-orientated thermal management model is then elucidated in Section 3. A brief review of the air flow compressor and the PEMFC stack models, which are used in building the integrated model, is provided in Appendix A. Subsequently, in Section 4, the results from simulation studies are presented with insights into the number of cooling plates, the knowledge of which is required during the design of the stack. Concluding remarks and directions for future work are given in Section 5.

2. Development of water pump model

A dynamic lumped parameter model is developed for the water pump with the objective of controlling the stack temperature by manipulating the coolant water flow rate. The coolant water flow rate can be manipulated in two different ways, namely: (i) by using a control valve in combination with a constant speed pump; (ii) by using a variable speed pump. The second arrangement is attractive since it does not involve the use of a valve and hence reduces the complexity and the weight of the system. In view of this, dynamic modelling of the variable speed centrifugal pump is taken up. The water flow rate of the pump is modelled as a function of motor-armature current and motor speed. The water pump model along with the thermal model facilitates a rigorous and realistic study of the stack temperature control problem. It is worth noting that the dynamics of the water pump have been neglected in earlier investigations pertaining to control of the stack temperature [12,13,16,18].

The dynamic pump model is developed based on the fundamental relationships between motor-armature current (input), motor speed and water flow rate (Q) (output) of the centrifugal pump reported by Kallesge [19]. The equations governing the relationships among the variables are

$$J_{\text{com}}\frac{d\omega_r}{dt} = \tau_e - B\omega_r - T_p \tag{1}$$

$$J_W\frac{dQ}{dt} = H_p - P_l \tag{2}$$

$$H_p = -a_1Q^2 + a_2Q\omega_r + a_3\omega_r^2 \tag{3}$$

$$T_p = -b_1Q^2 + b_2Q\omega_r + b_3\omega_r^2 \tag{4}$$

$$P_l = P_{\text{out}} - P_{\text{in}} + \rho g(z_{\text{out}} - z_{\text{in}}) - (K_v + K_p)Q^2 \tag{5}$$

where P_1, P_2, z_1, z_2 are the pressure and height values at the surface of the reservoir and the stack inlet, respectively.

The combined torque (τ_e) equation for a dc motor with varying armature current is given by [20]

$$\tau_e = CI_{\text{mot}} - \tau_f \tag{6}$$

The equation for load pressure provided above in Eq. (5) is modified for a centrifugal pump of constant head based on the following assumptions:

- No control valve is used to control the water flow rate; therefore, $K_v = 0$.
- Water in the reservoir is maintained at a constant level using stack coolant water recirculation.
- Water reservoir and pump outlet are opened to atmosphere; therefore, inlet pressure equals outlet pressure ($P_{\text{in}} = P_{\text{out}}$).
- Pressure drop across the stack is negligible.

The resulting form of Eq. (5) is

$$P_l = \rho g(z_2 - z_1) - K_pQ^2 \tag{7}$$

It is noted that Eq. (7) for the load pressure (P_l) contains two terms, namely: (i) pressure head ($g(z_2 - z_1)$) due to height (L); (ii) the pressure head due to pipe roughness (K_pQ^2) of length L.

Now, dividing Eqs. (1) and (2) by J_{com} and J_W, respectively, and then substituting Eqs. (3), (4), (6) and (7) for T_p, H_p, τ_e and P_l in Eqs.(1) and (2), yields

$$\frac{d\omega_r}{dt} = \frac{CI_{\text{mot}} - \tau_f}{J_{\text{com}}} + \tilde{B}\omega_r + \tilde{b}_1Q^2 + \tilde{b}_2Q\omega_r + \tilde{b}_3\omega_r^2 \tag{8}$$

$$\frac{dQ}{dt} = \tilde{a}_1Q^2 + \tilde{a}_2Q\omega_r + \tilde{a}_3\omega_r^2 - \frac{z_2 - z_1}{J_W} \tag{9}$$

Table 1
Parameters of Tuscan motor and Grundfos CR2-30 pump

Physical parameter	Value	Reference
C (N m A^{-1})	0.095	[20]
J ($\times 10^{-5}$ kg m^2)	2.7	[20]
τ_f (N m)	0.043	[29]
K_j ($\times 10^{-5}$ kg m^2) [a]	1.2	–

[a] Calculated for the casing volume and radius of 150 cm^3 and 4 cm, respectively.

Table 2
Comparison between experimental and predicted values of Grundfos CR2-30 motor-pump characteristic data

Current (A)	Experimental values		Predicted values	
	Speed (rps)	Flow rate (lps)	Speed (rps)	Flow rate (lps)
2.58	214	0.375	211	0.478
3.47	230	0.497	229	0.545
5.25	262	0.749	261	0.715
6.42	279	0.854	279	0.785
7.55	295	0.973	295	0.865

where $\tilde{B} = -B/J_{\text{com}}$, $\tilde{b}_1 = b_1/J_{\text{com}}$, $\tilde{b}_2 = -b_2/J_{\text{com}}$, $\tilde{b}_3 = -b_3/J_{\text{com}}$, $\tilde{a}_1 = K_p - a_1/J_W$, $\tilde{a}_2 = a_2/J_W$ and $\tilde{a}_3 = a_3/J_W$ are the modified coefficients; $(z_2 - z_1)$ is the distance (height) between the stack inlet and water surface of the reservoir and is assumed as 1 m.

The constants C, τ_f and J_{com} of this motor-pump are given in Table 1. The moment of inertia[1] of water (J_W) is calculated for a casing volume of 150 cm^3 (liquid volume = casing volume) and a radius of impeller of 4 cm, respectively. The modified coefficients in Eqs. (8) and (9) are obtained by simultaneously solving them at steady state. For this purpose, the input–output data of a Tuscan 36 V motor Grundfos CR2-30 centrifugal pump given in Table 2 are utilized. Five input–output data points are taken at different motor-pump speeds by discretizing the characteristic curves given in [20]. The estimated values of coefficients in Eqs. (8) and (9) are

$[\tilde{B} \quad \tilde{b}_1 \quad \tilde{b}_2 \quad \tilde{b}_3] = [0.09638 \quad 3.56801 \quad 0.02372 \quad -0.0006531] \times 10^3$

$[\tilde{a_1} \quad \tilde{a_2} \quad \tilde{a_3}] = [8.295961 \quad -0.060204 \quad 0.0001167] \times 10^5$

Simulation of the dynamic motor-pump model is performed using MATLAB-Simulink with the motor-armature current as input to the model. The motor-shaft speed and pump flow rate values obtained from the model are listed in Table 2 for comparison with the experimental values [20]. The results are in good agreement with the experimental values of shaft speed and pump flow rate. Later, this dynamic model along with the proposed stack thermal model is integrated with the PEMFC stack model for control studies. The thermal management model is described in the following section.

3. Thermal management model

A lumped parameter control-orientated thermal management model of a PEMFC stack is developed based on the energy balance discussed in Section 1. In this model, the heat loss to the surroundings is taken into account explicitly rather than being evaluated in an implicit form [16]. The developed thermal model can predict the temperature of the stack, the reactants at exit and the outlet coolant water for a given set of load (current), inlet coolant water and reactant flows.

[1] Mass × radius^2.

3.1. Control-orientated stack thermal model

The development of the thermal model is based on physico-chemical knowledge of the fuel cell stack and with following assumptions:

(1) the temperature is uniform over the whole length of the stack due to high thermal conductivity and the provision of a sufficient number of cooling plates in the stack;
(2) pure H_2 gas enters at the anode side of the stack;
(3) no liquid water enters at the anode and cathode sides;
(4) the formation of product water at the cathode is in vapour phase;
(5) water transport across the membrane is in the vapour phase only.

From the law of conservation of energy, the chemical energy of reactants H_2– O_2 equals the sum of the electrical energy of the fuel cell stack and the thermal energy generated due to overvoltage. This thermal energy is dispensed in the form of latent heat of vapourization of water at the cathode side, heat loss to the surroundings from the stack, and sensible heat of reactant gases and coolant water. The energy balance is given by

$$\dot{Q}_{\text{theo}} = \dot{Q}_{\text{elec}} + \dot{Q}_{\text{sens}} + \dot{Q}_{\text{latent}} + \dot{Q}_{\text{loss}} \tag{10}$$

The theoretical energy from the electrochemical reaction in a PEMFC is calculated by the product of the heat of reaction and the number of moles of the hydrogen consumed [21]. The associated equation is

$$\dot{Q}_{\text{theo}} = N_{\text{H}_2,\text{cons}}\,\Delta H_{\text{rxn}} \tag{11}$$

The electrical energy produced from the PEMFC stack with 'n' single cells is calculated as

$$\dot{Q}_{\text{elec}} = nV_{\text{cell}}I_{\text{st}} \tag{12}$$

The energy loss to the surroundings due to natural convection is calculated as

$$\dot{Q}_{\text{loss}} = h_{\text{st}}A_{\text{st}}(T_{\text{st}} - T_{\text{atm}}) \tag{13}$$

where an explicit form is used in contrast to the implicit form that was provided in [16] to account for the heat loss to the surroundings. The heat loss in the above equation is calculated using the value of the film heat transfer coefficient (h_{st}) obtained from the Nusselt number. The Nusselt number for a vertical plate has been derived by Churchil and Chu [22,23], i.e.

$$Nu = \frac{h_{\text{st}}L}{k} = \left[0.825 + 0.387\frac{Ra^{0.1333}}{[1+(0.492/N_{\text{pr}})^{0.56}]^{8/27}}\right]^2 \tag{14}$$

from which h_{st} is obtained.

The sensible heat of coolant water stream is calculated using the following formula where the loss of liquid mass by vapourisation is assumed to be negligible at the exit of the coolant water stream:

$$\dot{Q}_{\text{sens,W}} = N_{\text{W}}C_{p,\text{W}}(T_{\text{W,out}} - T_{\text{W,in}}) \tag{15}$$

From assumptions (2) and (3), the sensible heat at anode side is considered for two species, namely pure hydrogen and water vapour. The amount of liquid water on the anode side is neglected by virtue of a predominant electro-osmotic drag. Under these assumptions, the energy balance on anode is written as

$$\begin{aligned}\dot{Q}_{\text{sens,a}} = {} & N_{\text{H}_2,\text{a,out}}C_{p,\text{H}_2}(T_{\text{a,out}} - T_0) + N_{\text{W,v,a,out}}C_{p,\text{H}_2\text{O,v}}(T_{\text{a,out}} - T_0) \\ & - N_{\text{H}_2,\text{a,in}}C_{p,\text{H}_2}(T_{\text{a,in}} - T_0) - N_{\text{W,v,a,in}}C_{p,\text{H}_2\text{O,v}}(T_{\text{a,in}} - T_0)\end{aligned} \tag{16}$$

In the case of the dead end on the anode side as stated in Section 3.2, the species existing at anode side are zero despite the regular purging of hydrogen at the anode exit.

The sensible heat at the cathode side is considered for four species, namely: oxygen, nitrogen, water vapour and liquid water at the cathode exit. From assumptions (4) and (5), since the product water and the net water transport across the membrane are assumed to be in the vapour phase, the partial condensation of water vapour takes place on the cathode side. The condensation occurs when the partial pressure of water vapour reaches the saturation pressure at the stack temperature. The maximum water vapour that is held by the gas mixture is calculated as follows:

$$N_{\text{W,v,c,out,max}} = (N_{\text{O}_2,\text{c,out}} + N_{\text{N}_2,\text{c,out}})\frac{P^{\text{sat}}_{T_{\text{c,out}}}}{P_{\text{c,out}} - P^{\text{sat}}_{T_{\text{c,out}}}},$$

$$N_{\text{W,c,out}} = N_{\text{W,c,in}} + N_{\text{trans}} + N_{\text{W,prod}}$$

$$\text{If } N_{\text{W,c,out}} \gg N_{\text{W,v,c,out,max}}: \quad N_{\text{W,l,out}} = N_{\text{W,out}} - N_{\text{W,v,c,out,max}},$$

$$N_{\text{W,v,c,out}} = N_{\text{W,c,out,max}}$$

$$\text{If } N_{\text{W,c,out}} \le N_{\text{W,v,c,out,max}}: \quad N_{\text{W,l,out}} = 0, \quad N_{\text{W,v,c,out}} = N_{\text{W,c,out}}$$

The above equations along with the assumption that no liquid water enters at the cathode are used to write the sensible heat on cathode side as

$$\begin{aligned}\dot{Q}_{\text{sens,c}} = {} & N_{\text{O}_2,\text{c,out}}C_{p,\text{O}_2}(T_{\text{c,out}} - T_0) + N_{\text{W,v,c,out}}C_{p,\text{H}_2\text{O,v}}(T_{\text{c,out}} - T_0) \\ & + N_{\text{W,l,c,out}}C_{p,\text{H}_2\text{O,l}}(T_{\text{c,out}} - T_0) + N_{\text{N}_2,\text{c,out}}C_{p,\text{N}_2}(T_{\text{c,out}} - T_0) \\ & - N_{\text{O}_2,\text{c,in}}C_{p,\text{O}_2}(T_{\text{c,in}} - T_0) - N_{\text{W,v,c,in}}C_{p,\text{H}_2\text{O,v}}(T_{\text{c,in}} - T_0) \\ & - N_{\text{N}_2,\text{c,in}}C_{p,\text{N}_2}(T_{\text{c,in}} - T_0)\end{aligned} \tag{17}$$

Finally, the total sensible heat is computed as

$$\dot{Q}_{\text{sens}} = \dot{Q}_{\text{sens,a}} + \dot{Q}_{\text{sens,c}} + \dot{Q}_{\text{sens,W}} \tag{18}$$

The latent heat of water vapour due to phase change is calculated by noting that the molar flow rate of water involved during the phase change is the difference between the total water on the cathode side and the maximum water vapour that is held by the gas mixture ($N_{\text{W,v,c,out,max}}$):

If $N_{\text{W,c,out}} \gg N_{\text{W,v,c,out,max}}$:

$$\dot{Q}_{\text{latent}} = (N_{\text{W,c,out}} - N_{\text{W,v,c,out,max}})H_{\text{vapourisation}} \tag{19}$$

If $N_{\text{W,c,out}} \le N_{\text{W,v,c,out,max}}$:

$$\dot{Q}_{\text{latent}} = 0 \tag{20}$$

where $H_{\text{vapourisation}}$ is the latent heat of vapourization of water given by

$$\begin{aligned}H_{\text{vapourisation}} = {} & 45070 - 41.9T_{\text{st}} + 3.44\times10^{-3}T_{\text{st}}^2 + 2.54\times10^{-6}T_{\text{st}}^3 \\ & - 8.98\times10^{-10}T_{\text{st}}^4\end{aligned}$$

3.1.1. Calculation of stack temperature

The overall energy balance equation of fuel cell stack is given by

Energy accumulation = Energy in − Energy out

$$M_{\text{st}}C_{p,\text{st}}\frac{\text{d}T_{\text{st}}}{\text{d}t} = \dot{Q}_{\text{theo}} - (\dot{Q}_{\text{elec}} + \dot{Q}_{\text{sens}} + \dot{Q}_{\text{latent}} + \dot{Q}_{\text{loss}}) \tag{21}$$

Eq. (21) is vital to the calculation of the dynamic stack temperature where Eqs. (11), (12), (13), (18) and (19) are invoked to compute $\dot{Q}_{\text{theo}}$, $\dot{Q}_{\text{elec}}$, $\dot{Q}_{\text{loss}}$, $\dot{Q}_{\text{sens}}$ and $\dot{Q}_{\text{latent}}$, respectively.

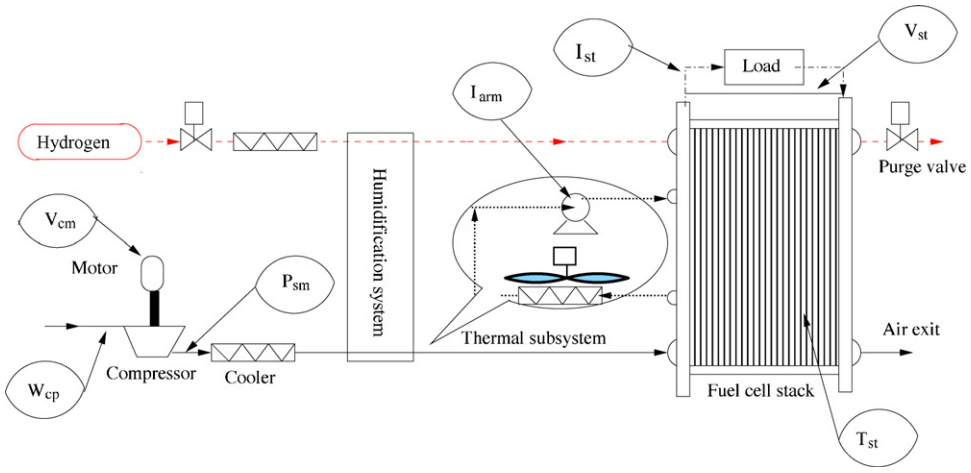

Fig. 1. Schematic of integrated PEMFC stack.

3.1.2. Calculation of coolant water outlet temperature

The outlet temperature of the coolant water ($T_{W,out}$) is calculated by equating the sensible heat of coolant water to the convective heat transfer of coolant water, i.e.

$$N_W C_{p,H_2O}(T_{W,out} - T_{W,in}) = h_W A_W (T_{LMTD}) \quad (22)$$

where the logarithmic mean temperature difference (T_{LMTD}) between cooling water and stack is used to represent the average temperature across the inlet and outlet of the stack and is given by

$$T_{LMTD} = \frac{T_{W,out} - T_{W,in}}{\ln((T_{st} - T_{W,in})/(T_{st} - T_{W,out}))} \quad (23)$$

After substituting for T_{LMTD} and by rearranging Eq. (22), the final expression for coolant outlet temperature takes the form:

$$T_{W,out} = T_{st} - \exp\left[\ln(T_{st} - T_{W,in}) - \frac{h_W A_W}{N_W C_{p,H_2O}}\right] \quad (24)$$

3.1.3. Calculation of cathode and anode exit gas temperatures

The temperatures of the exit gas flow streams at the anode and the cathode are calculated by equating the sensible heat of each gas mixture to the convective heat transfer of the gas mixture on each side (anode, cathode). The average exit temperatures of the gas mixture at the anode and the cathode, $T_{a,out}$ and $T_{c,out}$, are obtained using the expressions reported in [16]:

$$T_{a,out} = 2\left[T_{st} - \frac{Q_{sens,a} + Q_{mass,a}}{(hA)_a}\right] \quad (25)$$

$$T_{c,out} = 2\left[T_{st} - \frac{Q_{sens,c} + Q_{latent,c} - Q_{mass,c}}{(hA)_c}\right] \quad (26)$$

where $Q_{mass,a}$ and $Q_{mass,c}$ are the energy changes due to mass transfer and consumption of reactants at the anode and the cathode side, respectively, namely

$$\dot{Q}_{mass,a} = N_{trans} C_{p,H_2O,v}(T_{st} - T_0) + N_{H_2,con} C_{p,H_2}(T_{st} - T_0),$$

$$\dot{Q}_{mass,c} = N_{trans} C_{p,H_2O,v}(T_{st} - T_0) + N_{H_2,con} C_{p,H_2O,l}(T_{st} - T_0) - N_{O_2,con} C_{p,O_2}(T_{st} - T_0)$$

This completes the development of PEMFC stack thermal management model. The temperatures of the stack, the coolant outlet water and the anode and cathode exit streams can be obtained from Eqs. (21), (24), (25) and (26), respectively. The developed thermal model is now integrated with the PEMFC stack and air flow compressor models coded in MATLAB-Simulink environment [24] to carry out a study of the thermal effects on the PEMFC system. Due to the result of thermal model integration, an input (motor-pump current) and output (stack temperature) are added in addition to the input (compressor motor voltage) and output (air flow rate) of the PEMFC stack and air flow compressor models. The equations describing the PEMFC stack and the air flow compressor are provided in Appendix A. A schematic of the integrated model is shown in Fig. 1. Further, this integrated model is used for interaction analysis, as discussed in Section 4.4. An overview of the PEMFC system with which the thermal model is integrated is given below for convenience.

3.2. Review of PEMFC stack model

Pukrushpan et al. [17] have developed a system level lumped parameter model based on physical-chemical knowledge of the processes involved in the PEMFC stack and its reactant (air) supply system [17,25]. It contains the air flow compressor model and the semi-empirical current–voltage model (i.e. polarization curve). This model is employed to maintain the oxygen excess ratio at the desired value of 2 when the stack is subjected to dynamic load changes. The salient features and the underlying assumptions of this model are as follows:

- The parameters used in PEMFC stack model are based on the 75 kW stack used in the FORD P2000 fuel cell prototype vehicle.
- A semi-empirical model of the current–voltage curve is built based on a wide range of stack operating temperature (50–90 °C) data.
- The stack comprises 381 cells of active area 280 cm^2.
- The humidity of the reactant gases is constant.
- The fuel (H_2) supply on anode side is considered to be static and only the air flow rate dynamics are considered.
- Hydrogen is supplied at the anode side in stoichiometry proportion and is adjusted instantaneously with a proportional control valve placed at the high-pressure cylinder.
- The dead end is considered at the anode exit.
- The temperature of the stack is assumed to be constant at 80 ° C and is uniform over the whole length of the stack.
- All gases are assumed to possess ideal gas behaviour.
- The temperature on the cathode flow channel is assumed to be equal to the stack temperature.

Table 3
Parameters to be supplied to simulate integrated stack model

Variable	Value	Reference
Physical data		
L (m)	0.805	[30]
A_{st} (m^2)	1	[30]
A_{an} (m^2)	2	[25][a]
A_{ca} (m^2)	8	[25][a]
A_W (m^2)	0.034/plate	[30][a]
$(MC_p)_{st}$ (kJ K^{-1})	35 × 15	[16]
Physical parameters		
h_c (W m^{-2} K^{-1})	25	[31]
h_a (W m^{-2} K^{-1})	25	[31]
h_W (W m^{-2} K^{-1})	720	[21]
C_{p,H_2} (J mol^{-1} K^{-1})	28.82	[21]
C_{p,O_2} (J mol^{-1} K^{-1})	29.38	[21]
C_{p,N_2} (J mol^{-1} K^{-1})	29.12	[21]
C_{p,H_2O_v} (J mol^{-1} K^{-1})	36.24	[21]
C_{p,H_2O} (J mol^{-1} K^{-1})	77.22	[21]
ν ($\times 10^{-5}$ m^2 s^{-1})	1.868	[21]
K_{air} (W m^{-1} K^{-1})	0.029	[21]
Operating values of the stack		
T_{atm} (K)	298.15	
$T_{a,in}$ (K)	333.15	
$T_{c,in}$ (K)	328.15	
$T_{W,in}$ (K)	318.15	
$RH_{c,in}$, $RH_{a,in}$	1	

[a] Area of anode, cathode and single cooling plate are calculated based on Mark902 Ballard stack data.

3.3. Simulation of integrated model

Additional parameters introduced due to the integration of the thermal model are set to the values given in Table 3. The settings for the air flow compressor and voltage–current model are set to their suggested values [17]. The inputs required to simulate the stack thermal model are the molar flow rates of hydrogen, oxygen, nitrogen, water streams, water transport across the membrane and total pressure at the cathode exit, and electrical energy generated from stack. These inputs are taken from the anode, the cathode, the membrane hydration and current–voltage models of the PEMFC stack and air flow compressor model.

4. Results and discussion

The developed thermal model is validated based on the results of Ballard V 5 kW thermal data available in the literature [26]. Due to the non-disclosure of Ballard 900 stack[2] data, the input conditions of 5 kW Ballard stack are scaled-up to facilitate the comparison with the results from the simulation of the 70 kW stack under consideration. The scaling is done by maintaining similar temperatures of coolant water and inlet feeds at the anode and the cathode. Table 4 provides this information along with the values of the physical data used for validating the model. Further, the stack heat capacity, oxygen and inlet coolant water flow rates of the 5 kW unit [26] are scaled by factor of 14. The inlet hydrogen flow rate at the anode is taken as per stoichiometry. The aforementioned variables are linearly scaled based on the assumption that the polarization curves of both Ballard V (5 kW) and Ballard 900 (70 kW) stacks are similar. This assumption is valid since the same membrane (Nafion-117) is used in both the stacks.

The stack and exit temperatures of the outlet streams of the 70 kW stack would be equivalent to those of the 5 kW stack, provided the thermal energy released from 70 kW stack equals 14 times the thermal energy released from the 5 kW stack. The amount of load required to generate this thermal energy is calculated as

$$E_{chemical} - E_{electrical} = 14 \times (E_{chemical} - E_{electrical}) \quad (27)$$

$$381 \times I_{st} \left(\frac{\triangle H}{2F} - 0.82 \right) = 14 \times 35 \times 20 \left(\frac{\triangle H}{2F} - 0.82 \right) \quad (28)$$

Further, the parameters ($(hA)_a$, $(hA)_c$, $(hA)_W$) of 70 kW stack are obtained by linearly scaling the Ballard V (5 kW) stack values. The heat capacity ($M_{st}C_{p,st}$) of the 70 kW stack is taken as 14 times that of the 5 kW stack to facilitate the same settling time as that of the 5 kW stack temperature. To validate the developed model with the experimental values, the data given in Table 4 is used instead of the corresponding same parameters given in Table 3.

The heat transfer coefficient (h_{st}) between the air and the stack surfaces is calculated using Eq. (14) and is shown in Fig. 2. The resulting values are found to be in the range of the experimental values (3–7 W m^{-2} K^{-1}) given in [27] when the stack is operated between 50 and 90 °C. The steady-state temperatures of the stack, coolant water and cathode outlet of the 70 kW stack obtained from the simulation of the developed thermal model are shown in Table 5 for the same inlet temperatures of the coolant water and the reactants as that of the 5 kW stack. The last column of this table contains the corresponding outputs of the 5 kW for the pur-

Table 4
Table of Ballard V (5 kW) and scaled data of 70 kW (Ballard 900) for similar inputs

Stream	Parameters	Value (5 kW)	Value (70 kW)
Inlet anode gas	$N_{H_2,a,in}$ (mol s^{-1})	0.0078	0.0508
	$T_{a,in}$ (K)	296.65	296.65
Inlet cathode gas	$N_{O_2,c,in}$ (mol s^{-1})	0.004	0.0560
	$T_{c,in}$ (K)	296.65	296.65
Inlet water	$N_{W,in}$ (mol s^{-1})	1.84	25.76
	$T_{W,in}$ (K)	296.65	296.65
Other data	$(MC_p)_{st}$ (kJ K^{-1})	35	490
	$(hA)_a$ (W K^{-1})	2	28
	$(hA)_c$ (W K^{-1})	10	140
	$(hA)_W$ (W K^{-1})	50	700
	T_{room} (K)	296.65	296.65
	n_{cells}	35	381
	I (A)	20	25.7
	$RH_{a,in}$	1	1
	$RH_{c,in}$	1	1

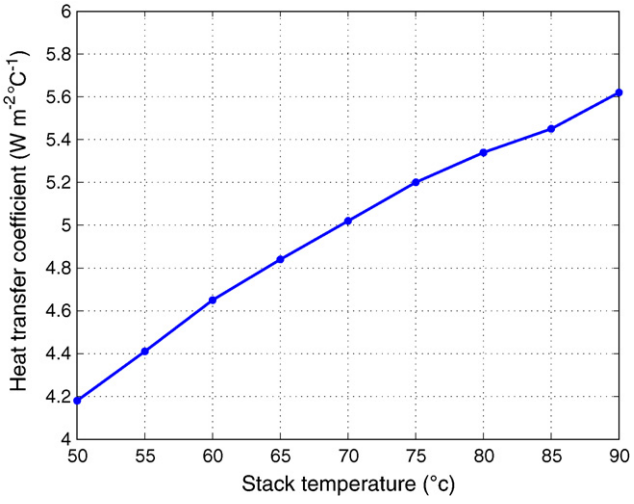

Fig. 2. Free convective heat transfer coefficient from stack to surroundings.

[2] Peak power of the stack is 70 kW and the latter contains 381 cells of active area 280 cm^2.

Table 5
Validation of thermal model with Ballard V (5 kW) temperature data

Stream	Parameter	predicted value	Experimental value
Outlet anode gas	$T_{a,out}$ (K)	Dead end	298.65
Outlet cathode gas	$T_{c,out}$ (K)	312.41	311.95
Outlet water	$T_{W,out}$ (K)	299.42	297.05
Other data	T_{st} (K)	306.11	311.15
	V_{cell} (V)	0.76	0.81
	t [a] (min)	60	55

[a] Settling time of stack temperature.

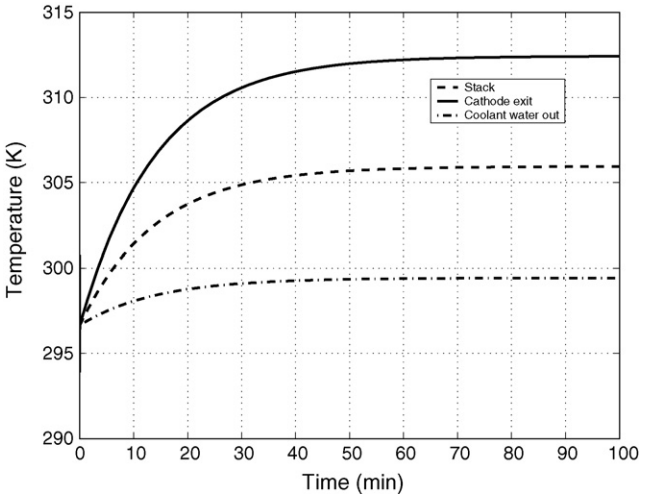

Fig. 3. Dynamic temperature of stack and outlet streams at 25.7 A load.

pose of comparison. It is seen that the predicted values match well with the experimental data. The transient temperature responses of the stack, cathode and coolant outlet streams are shown in Fig. 3. It is inferred from Fig. 3 that the settling time of the stack temperature is 60 min while that of the Ballard V stack is 55 min. The discrepancy between experimental and predicted temperatures and the settling time is due to the difference in cell voltages of the 5 and 70 kW stacks which is assumed to be constant during the load calculation. The temperature of the anode exit gas is not reported here due to the dead-end configuration of the 70 kW stack, as stated in Section 3.2, which is open-end in the 5 kW Ballard V stack.

The results of the pump model validation were presented in Section 2. Thus the proposed model provides predictions that are concurrent with the physics of the process as reported in the literature. The thermal model, water pump model and the existing PEMFC stack model are integrated, as described in Section 3.3. This integrated model is used to examine the effect of (i) the number of cooling plates on the coolant outlet temperature and (ii) the stack heat capacity on the settling time of the stack temperature. The load current and compressor motor voltage are set to 191 A and 164 V, respectively, and result in a net power[3] of 40 kW [25]. The stack is operated at 353.15 K. The motor-armature current of the water pump is set to 1.157 A to ensure that the stack temperature is maintained at 353.15 K. The parameters given in Table 3 are used in conjunction with these operating conditions. Further, the effect of stack temperature on the settling times of air flow, the stack voltage, the net power and the oxygen excess ratio under closed-loop operation is studied.

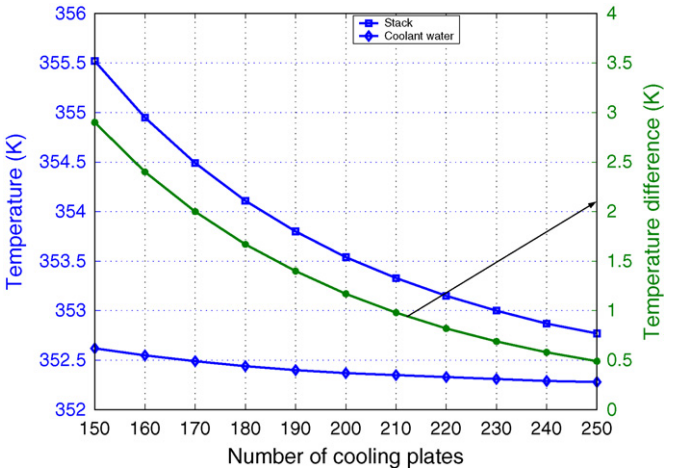

Fig. 4. Effect of number of cooling plates on exit coolant water temperature.

4.1. Influence of number of cooling plates on exit coolant water temperature

The main advantage of this study is that the parasitic losses due to auxiliary equipment like radiators can be reduced. These radiators are used to cool the outlet coolant water to a reasonable low temperature before it is fed back at the stack inlet.

The number of cooling plates that are chosen for this study are in the range of n /4 to 3n /4, where 'n' is the number of single cells in the stack. From Fig. 4 it is observed that the temperature of the coolant outlet reaches close to that of the stack, i.e. the temperature difference between the stack and the coolant outlet water is 1 °C or below as the number of cooling plates is increased beyond 220. A further increase in the number of cooling plates leads to only a marginal decrease in the temperature difference at the expense of increase in weight and size of the system. In view of these observations, the number of cooling plates is fixed at 220 for subsequent studies.

4.2. Influence of stack heat capacity on settling time of stack temperature

Eq. (21) describes the dynamic relationship of stack temperature with M_{st} and $C_{p,st}$. Simulation studies are conducted to *quantify* the influence of mass (M_{st}) and average specific heat capacity ($C_{p,st}$) of the stack on the settling time of the stack temperature which, in turn, effects the stack start-up time.

The settling time of the stack temperature is studied by gradually decreasing the heat capacity quantity, i.e. $(MC_p)_{st}$, below the nominal value of the 70 kW stack.[4] The heat capacity can be varied by choosing materials alternative to graphite for bipolar or cooling plates that result in lower values of $(MC_p)_{st}$. From Fig. 5, it is observed that the settling time of the stack temperature decreases almost linearly with decrease in the stack heat capacity, as expected. Based on this observation, fuel cells of today are built using a lower heat capacity than graphite. Coated bipolar plates and cooling flow-field plates made out of aluminum possess higher thermal and electrical conductivity than graphite in addition to a low heat capacity. Therefore, aluminum can be preferred for making bipolar (coated) and cooling plates. This study has been carried out

[3] Net power = stack power − power drawn by the air compressor.

[4] The product of $(MC_p)_{st}$ is taken as 490 kJ K^{-1} based on the Ballard 5 kW stack.

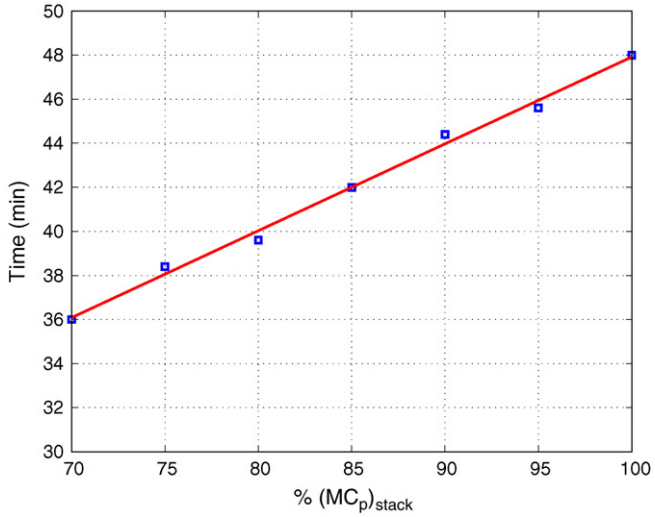

Fig. 5. Effect of heat capacity of stack on settling time of stack temperature.

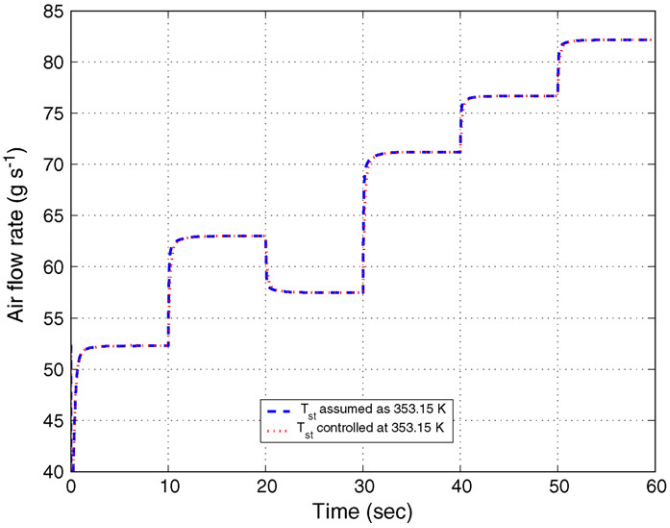

Fig. 7. Dynamic response of air flow rate under various load conditions.

on the lines of quantifying the influence of the material on the settling times of stack temperature as this which is important during start-up of the stack.

4.3. *Effect of stack temperature on air flow compressor, stack voltage, oxygen excess ratio and net power transients*

To investigate these effects, studies are conducted under two different conditions, namely: (i) constant temperature (as per the assumption made in [25] and re-stated in Section 3.2) and (ii) temperature is controlled at a desired value (353.15 K). The difference between these two conditions is that in the second case, the stack temperature and the controller dynamics are taken into account. The results obtained for both the cases are discussed below.

The abovementioned cases are studied in a closed loop with the same load (current) profile as given in [17] and shown in Fig. 6. In the first case (constant temperature), a PI controller is employed to control the air flow rate such that an oxygen excess ratio of two is maintained. The integrated model is used to simulate the second case where temperature dynamics are taken into consideration. Here, two single-loop PI controllers are used to control the air flow rate and stack temperature separately by manipulating the compressor motor voltage and motor-armature current, respectively. The resulting settling times of outputs (voltage, air flow rate) and performance variables (oxygen excess ratio, net power) are compared for both cases.

The dynamic response of the air flow rate, oxygen excess ratio, stack voltage, net power and stack temperature are shown in Figs. 7–11 , respectively. It is observed from Figs. 7 and 8 that the air flow rate and oxygen excess ratio settle within 4 s in both cases. On the other hand, it can be noticed from Fig. 9 that the stack voltage shows a significant bias when compared with the results of the constant-temperature case where it settles within 5 s. The shift in voltage away from the steady-state value due to temperature change can be expected to result in a bias in the stack net power when compared with the constant temperature case, as shown in Fig. 10. The difference in the net power output is in the range of 250–300 W, which may not be discernible due to the scaling that is used to display the net power (in kW). The bias in voltage is due to the fact that the voltage is a function of stack temperature which does not settle within the duration spanned by two successive load changes, the stack temperature and the corresponding input motor-armature current profiles are shown in Fig. 11. This is associated with the fact that the open-loop settling time of the stack temper-

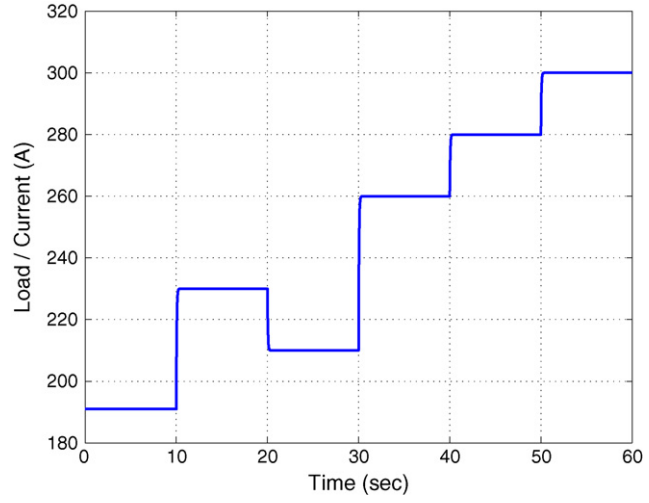

Fig. 6. Load profile used in [17] at different times of interval.

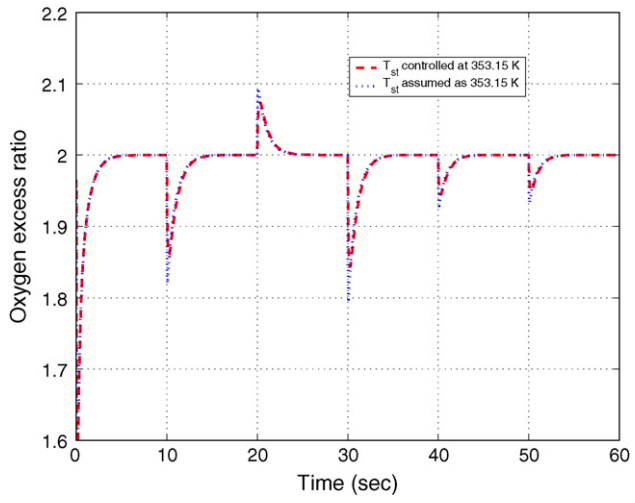

Fig. 8. Oxygen excess ratio during dynamic load conditions.

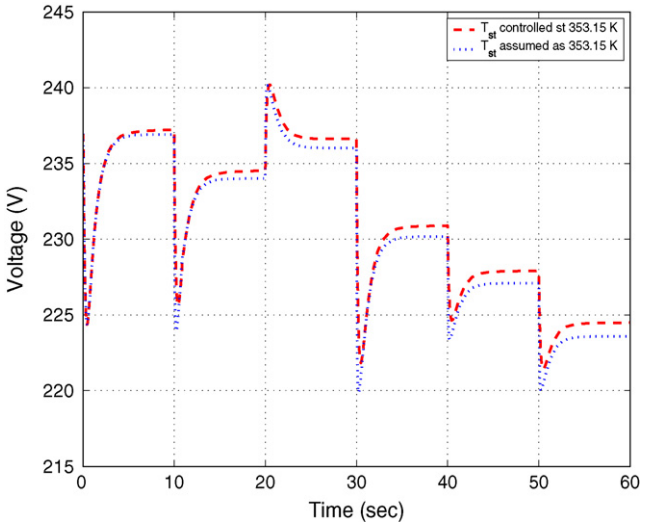

Fig. 9. Dynamic response of stack voltage under various load conditions.

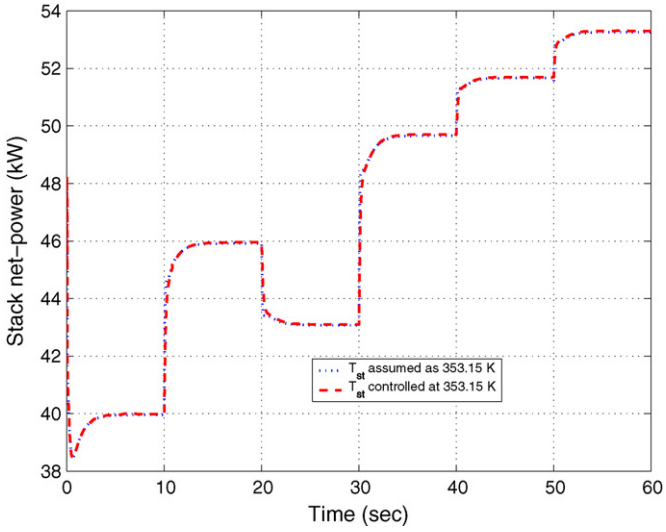

Fig. 10. Net power during dynamic load conditions.

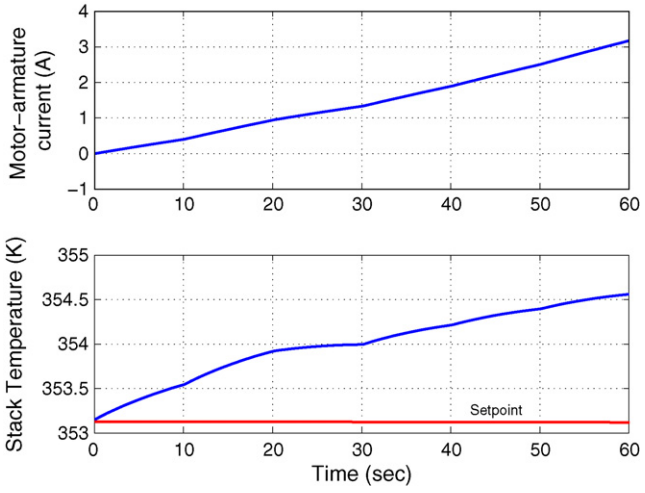

Fig. 11. Profiles of motor armature current (manipulated) and stack temperature (controlled) when controlled at 353.15 K.

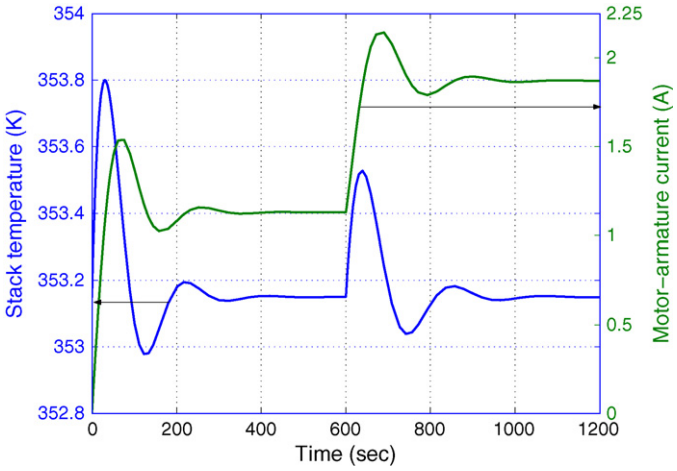

Fig. 12. Closed-loop settling time of stack temperature for step-change in load from 191 to 230 K.

ature is about 50 min (3000 s) and therefore it is only reasonable to design a controller that can result in closed-loop settling times greater than 5 min (1/10th of open-loop settling time). In fact, with the tunings used in the simulations the settling time of the stack temperature is 6 min (nearly 300 s) as shown in Fig. 12 for a step change in load (191–230 A).

Since the air flow is one of the carriers of thermal energy from the stack, it influences the stack temperature. By contrast, the effect of the stack temperature on the compressor air flow is virtually non-existent. In order to quantify the extent of interactions among the input–output pairs, interaction studies are conducted using the Relative Gain Array (RGA) tool. The results are presented in the following section.

4.4. Interaction studies—from a control perspective

The primary objective of this study is to assess the extent of interaction for control purposes. The steady-state interaction between inputs (compressor motor voltage and motor-pump current) and outputs (air flow rate and stack temperature) of interest are studied using the integrated model built in a MATLAB-Simulink environment. The interaction between each input–output pair is facilitated by the well-known RGA analysis [28], i.e.

$$\mathrm{RGA} = \begin{matrix} \\ y_1 \\ y_2 \end{matrix} \begin{matrix} \begin{matrix} u_1 & u_2 \end{matrix} \\ \begin{bmatrix} 1.078 & -0.074 \\ -0.079 & 1.062 \end{bmatrix} \end{matrix}$$

The RGA matrix suggests that the pairs output 1 (y_1: air flow rate)–input 1 (u_1: compressor motor voltage) and output 2 (y_2: stack temperature)–input 2 (u_2: motor-pump current) have a strong interaction. On the other hand, the off-diagonal pairs, namely, input 1–output 2 and input 2–output 1 exhibit very weak interaction. Therefore, it is concluded that the loops can be controlled on an individual basis.

5. Conclusions

In this investigation, a control-orientated thermal management model together with a dynamic water pump model has been developed to predict the temperatures of the stack, cathode, anode and

coolant exit streams for changes in air flow compressor voltage, coolant water flow rate (motor-pump armature current) and load conditions. The practical utility of these models has been demonstrated by integrating them with PEMFC stack current–voltage and air flow compressor models that exist in the literature.

The results obtained from the simulation studies of the integrated system showed good agreement with the experimental data available in the literature. Further, these results were shown to be useful in obtaining good physical insights into (i) the choice of alternative materials for cooling plates and bipolar plates other than graphite that can reduce the settling time of the stack temperature and the overall size of the PEMFC system, and (ii) the required number of cooling plates to ensure that the temperature of the coolant outlet water is close to that of the stack.

The open-loop study of the thermal subsystem showed that the settling time of the temperature is about 50 min, for a step-change in the load. The closed-loop system is tuned such that the stack temperature settles in about 6 min. Interaction studies were carried out to analyze the effect of the thermal sub-system on the air flow rate sub-system and *vice versa*. These studies revealed that the settling times of most of the variables remain unaffected due to the dynamics of the temperature loop, while the voltage and net power settle only after the temperature settles down. The implication of this fact from a control perspective is that the two sub-systems can be treated as non-interacting systems suggestive of the use of single-loop controllers for each of these loops.

The integrated model developed in this paper is useful in a few important aspects. For instance, it can be employed to study process heat integration and disturbance (load) rejection to avoid oxygen starvation and system faults detection and diagnosis. Further, various control algorithms can be tested using this model for maintaining the stack temperature. Advanced control schemes may be required to minimize the settling times of the air flow rate and to minimize the fluctuations in the stack temperature. These issues provide directions for future studies.

Appendix A

A.1. Brief overview of compressor and polarization curve model

The PEMFC stack system contains the models of the fuel cell stack and its auxiliary components such as compressor model, manifold model and humidification model [17,25].

Compressor model. The inputs to the model include inlet air pressure $p_{cp,in}$, its temperature $T_{cp,in}$, the voltage command to the compressor motor v_{cm}, and downstream pressure p_{sm}. The only dynamic state in this model is compressor speed ω_{cp}. The torque required to drive the compressor is given by

$$\tau_{cp} = \frac{C_p}{\omega_{cp}} \frac{T_{atm}}{\eta_{cp}} \left[\left(\frac{p_{sm}}{p_{atm}} \right)^{(\gamma-1)/\gamma} - 1 \right] W_{cp} \tag{A.1}$$

The dynamic behaviour of the compressor speed is represented by

$$J_{cp} \frac{d\omega_{cp}}{dt} = (\tau_{cm} - \tau_{cp}) \tag{A.2}$$

The compressor motor torque is calculated as

$$\tau_{cm} = \eta_{cm} \frac{C}{R_{cm}} (v_{cm} - k_v \omega_{cp}) \tag{A.3}$$

where C, R_{cm} and k_v are motor constants and η_{cm} is motor mechanical efficiency.

Supply manifold. The inlet mass flow is compressor air flow W_{cp} and the outlet mass flow is $W_{sm,out}$. State equations are

$$\frac{dm_{sm}}{dt} = W_{cp} - W_{sm,out} \tag{A.4}$$

$$\frac{dp_{sm}}{dt} = \frac{\gamma R_a}{V_{sm}} (W_{cp} T_{cp,out} - W_{sm,out} T_{sm}) \tag{A.5}$$

where V_{sm}, γ, R_a and T_{sm} are the supply manifold volume, specific heat, ideal gas constant and supply manifold temperature of air, respectively.

Humidifier (static) model. Before the air is fed into the humidifier, it is cooled to a desired temperature in the static cooler. $W_{v,cl}$ is the amount of water vapour present in the air–water vapour mixture before the air is humidified. $W_{v,hm}$, $p_{v,hm}$ and ϕ_{hm} are the vapour flow rate, vapour pressure and relative humidity of the gas mixture at the humidifier exit as follows:

$$W_{v,hm} = W_{v,cl} + W_{v,inj} \tag{A.6}$$

$$p_{v,hm} = \frac{W_{v,hm}}{W_{a,cl}} \frac{M_a}{M_v} p_{a,cl} \tag{A.7}$$

$$\phi_{hm} = \frac{p_{v,hm}}{p_{sat}(T_{hm})} \tag{A.8}$$

where $W_{v,inj}$ is the amount of water vapour injected in the humidifier, $W_{a,cl}$ the dry flow rate of air, $p_{a,cl}$ the partial pressure of dry air, T_{hm} the temperature of humidifier, and M_a and M_v are the molecular mass of air and water vapour, respectively.

Similar equations are used on hydrogen side.

Cathode flow model. The model is developed using the mass conservation principle and thermodynamic and psychometric properties of air. The flow model is lumped as a CSTR, i.e. the variables at cathode exit, namely, temperature $T_{ca,out}$, pressure $p_{ca,out}$ and oxygen mole fraction $y_{O_2,ca,out}$ are assumed to be the same as the they are in the cathode flow channel, T_{ca}, p_{ca} and $y_{O_2,ca}$. The mass continuity equations are

$$\frac{dm_{O_2,ca}}{dt} = W_{O_2,ca,in} - W_{O_2,ca,out} - W_{O_2,reacted} \tag{A.9}$$

$$\frac{dm_{N_2,ca}}{dt} = W_{N_2,ca,in} - W_{N_2,ca,out} \tag{A.10}$$

$$\frac{dm_{W,ca}}{dt} = W_{v,ca,in} - W_{v,ca,out} + W_{v,ca,gen} + W_{v,membr} - W_{l,ca,out} \tag{A.11}$$

Return manifold. The return manifold pressure at the cathode is modelled by

$$\frac{dp_{rm}}{dt} = \frac{R_a T_{rm}}{V_{rm}} (W_{ca,out} - W_{rm,out}) \tag{A.12}$$

where V_{rm} is the return manifold volume and T_{rm} is the temperature of the gas in the return manifold.

Anode flow model. Assumptions are similar to the cathode flow models. The hydrogen is compressed and stored in a hydrogen tank and the anode inlet flow rate is assumed to be supplied instantaneously with a valve of a fast actuator to maintain a minimum pressure difference between the anode and the cathode. The state equations are

$$\frac{dm_{H_2,an}}{dt} = W_{H_2,an,in} - W_{H_2,an,out} - W_{H_2,reacted} \tag{A.13}$$

$$\frac{dm_{W,an}}{dt} = W_{v,an,in} - W_{v,an,out} - W_{v,membr} - W_{l,an,out} \tag{A.14}$$

Membrane hydration model. This calculates the water content in the membrane and rate of mass flow across the membrane. Both

water content and mass flow are assumed to be uniform over the surface area of the membrane. The membrane water content and the rate of mass flow across the membrane are functions of the stack current and relative humidity of the reactants in the anode and the cathode flow channels.

Water transport across the membrane is considered to occur in two ways, namely: (i) electro-osmotic drag where the water molecules are dragged from the anode to the cathode side by protons; (ii) back diffusion, in this case the water molecules are transferred due to the concentration gradient of water across the membrane. The expressions are as follows:

$$N_{\mathrm{v,osmotic}} = n_{\mathrm{d}} \frac{i}{F}, \quad N_{\mathrm{v,diff}} = -D_{\mathrm{W}} \frac{c_{\mathrm{v,ca}} - c_{\mathrm{v,a}}}{t_{\mathrm{m}}}$$

The net transport of water across the membrane is given by

$$N_{\mathrm{v,membr}} = N_{\mathrm{v,osmotic}} + N_{\mathrm{v,diff}} \tag{A.15}$$

where $N_{\mathrm{v,osmotic}}$ ($\mathrm{mol\,s^{-1}\,cm^{-2}}$) is the net water flow from anode to cathode of one cell caused by electro-osmotic drag, i ($\mathrm{A\,cm^{-2}}$) the stack current density, F the Faraday number and n_{d} the electro-osmotic drag coefficient, $N_{\mathrm{v,diff}}$ ($\mathrm{mol\,s^{-1}\,cm^{-2}}$) the net water flow from cathode to anode of one cell caused by back-diffusion, c_{v} ($\mathrm{mol\,cm^{-3}}$) the water concentration, t_{m} the thickness of the membrane (cm) and D_{W} ($\mathrm{cm^2\,s^{-1}}$) is the diffusion coefficient of water in the membrane.

Stack voltage model. The voltage is calculated using a combination of physical and empirical relationships, and is given by

$$v_{\mathrm{fc}} = E - v_{\mathrm{act}} - v_{\mathrm{ohm}} - v_{\mathrm{conc}} = E - [v_0 + v_{\mathrm{a}}(1 - \mathrm{e}^{-c_1 i})] - [iR_{\mathrm{ohm}}] - \left[i\left(c_2 \frac{i}{i_{\max}} \right)^{c_3} \right] \tag{A.16}$$

where E is the open-circuit voltage, v_{act}, v_{ohm} and v_{conc} are the voltage drops due to activation loss, ohmic loss and concentration loss, respectively. The open-circuit voltage is calculated using the energy balance between the reactant and products, and the Faraday constant. It is given by

$$E = 1.229 - 8.5 \times 10^{-4}(T_{\mathrm{st}} - 298.15) + 4.3085 \times 10^{-5} T_{\mathrm{st}} [\ln(p_{\mathrm{H_2}}) + 0.5 \ln(p_{\mathrm{O_2}})] \tag{A.17}$$

where v_0 (V) is the voltage drop at zero current density, i the current density ($\mathrm{A\,cm^{-2}}$), R_{ohm} the internal electrical resistance ($\Omega\,\mathrm{cm^2}$), and v_{a}, $i_{\max}$, c_1, c_2 and c_3 are constants. The parameters in the expression (A.16) are determined using nonlinear regression of fuel cell polarization data from an automotive propulsion-sized fuel cell stack. The results obtained from the model show good accuracy when it is tested at an operating temperature between 40 and 100 °C and for various cathode pressures.

References

[1] J.C. Amphlett, R.M. Baumert, R.F. Mann, B.A. Pepply, P.R. Roberge, J. Power Sources 49 (1994) 349–356.
[2] R. Andrew, Li, J. Power Sources 102 (2001) 82–96.
[3] Y.J. Zhang, M.G. Ouyang, J.X. Luo, Y.J. Wang, Mathematical modeling of vehicle fuel cell power system thermal management, SAE Pap. 1 (2003) 11–46.
[4] V. Gurau, H. Liu, S. Kakac, AIChE J. 44 (1998) 2410–2422.
[5] T. Berning, D.M. Lu, N. Djilali, J. Power Sources 106 (2002) 284–294.
[6] T. Berning, N. Djilali, J. Power Sources 124 (2003) 440–452.
[7] K. Haraldsson, K. Wipke, J. Power Sources 126 (2004) 88–97.
[8] D. Cheddie, N. Munroe, J. Power Sources 147 (2005) 72–84.
[9] G. Maggio, V. Recupero, L. Pino, J. Power Sources 101 (2001) 275–286.
[10] L. Pisani, G. Murgia, M. Valentini, B. D'Aguanno, J. Power Sources 108 (2002) 92–203.
[11] A.R. Maher, S. Al-Baghdadil, Renew. Energy 30 (2005) 1587–1599.
[12] Y. Zhang, M. Ouyang, Q. Lu, J. Luo, X. Li, Appl. Therm. Eng. 24 (2004) 501–513.
[13] Y. Shan, S.-Y. Choe, J. Power Sources 158 (2006) 274–286.
[14] K.B. Wipke, M.R. Cuddy, S.D. Burch, Advisor 2.1: A User-Friendly Advanced Powertrain Simulation Using a Combined Backward/Forward Approach, Technical Report nrel/ja-540–26839, NREL, 1999.
[15] C.N. Maxoulis, D.N. Tsinoglou, G.C. Koltsakis, Energy Convers. Manage. 45 (2004) 559–573.
[16] X. Yu, B. Zhou, A. Sobiesiak, J. Power Sources 147 (2005) 184–195.
[17] J.T. Pukrushpan, H. Peng, A.G. Stefanopoulou, J. Dyn. Syst. Meas. Control 126 (2004) 14–25.
[18] X. Li, G. Cao, X. Zhu, Energy Convers. Manage. 47 (2006) 1032–1050.
[19] C.S. Kallesge, R.I. Zamanabadi, H.R. Vincent Cocquempot, in: International Conference on Control Applications, Taipei, Taiwan, September 2–4, 2004. IEEE Transactions.
[20] H. Suehrcke, J. Appelbaum, B. Reshef, Solar Energy 59 (1–3) (1997) 37–42.
[21] F. Frano, PEM Fuel Cells: Theory and Practice, Elsevier Academic Press, 2005.
[22] F.P. Incropera, D.P. DeWitt, Fundamental of Heat and Mass Transfer, 4th ed., Wiley-VCH, 1996.
[23] C. Graf, A. Vath, N. Nicoloso, J. Power Sources 155 (2006) 52–59.
[24] http://www.springer.com/west/home/engineering?SGWID=4–175-22–29400120-0.
[25] J.T. Pukrushpan, A.G. Stefanoupoulou, H. Peng, Control of fuel cell power systems: principles, modeling, analysis and feedback design, Advances in Industrial Control, Springer, 2004.
[26] J.C. Amphlett, B.A. Peppley, R.F. Mann, P.R. Roberge, A. Rodrigues, J. Power Sources 61 (1996) 183–188.
[27] J.H. Koh, A.T. Hsu, H.U. Akay, M.F. Liou, J. Power Sources 144 (2005) 122–128.
[28] G. Stefhanopoulos, Chemical Process Control—An Introduction to Theory and Practice, Prentice Hall, India, 2004.
[29] W. Anis, T. Kerbache, R. Mertens, R. Van Overstraeten, Solar Wind Technol. 1 (4) (1984) 197–205.
[30] Ballard Power Systems Inc., Mark902 Fuel Cell Module Specifications, 2005, http://www.ballard.com.
[31] T.V. Nguyen, R.E. White, J. Electrochem. Soc. 140 (8) (1993) 2178–2186.